Structural Characterization of Highly Oriented Naphthalene-Diimide-Bithiophene Copolymer Films via Vibrational Spectroscopy

Ester Giussani,[†,‡] Luigi Brambilla,[‡] Daniele Fazzi,*[,§] Michael Sommer,[∥] Navaphun Kayunkid,[⊥] Martin Brinkmann,[⊥] and Chiara Castiglioni*[,‡]

[†]Center for NanoScience and Technology CNST, IIT@PoliMi, via Pascoli 70/3, 20133 Milano, Italy

[‡]Dipartimento di Chimica, Materiali e Ing. Chimica, CMIC, "G. Natta", Politecnico di Milano, p.zza Leonardo da Vinci, 20133 Milano, Italy

[§]Max-Planck-Institut für Kohlenforschung (MPI-KOFO), Kaiser-Wilhelm-Platz 1, 45470 Mülheim an der Ruhr, Germany

[∥]Institute for Macromolecular Chemistry, University of Freiburg, Stefan-Meier-Strasse 31, 79104 Freiburg, Germany

[⊥]Institut Charles Sadron, CNRS − Université de Strasbourg, 23 Rue du Loess, 67034 Strasbourg, France

1. INTRODUCTION

Organic semiconducting polymers gained increasing importance in electronic and optical applications, providing a technology complementary to that based on silicon or other inorganic semiconductors.[1−16] Materials of p-type have been extensively studied in the past decade, and hole mobilities reaching 10−20 $cm^2\ V^{-1}\ s^{-1}$ have been obtained for small molecules and conjugated polymers.[10,17] On the other hand, the synthesis of n-type materials still remains a challenge due to their high reactivity with water and oxygen.[18]

Rylene diimide-based copolymers[19−22] and especially naphthalene diimide copolymers[23] exhibit good air stability and high electron affinity. In 2009, Facchetti et al.[24,25] reported the synthesis of a high performance n-type copolymer, poly{[*N*,*N*′-bis(2-octyldodecyl)-naphthalene-1,4,5,8-bis(dicarboximide)-2,6-diyl]-*alt*-5,5′-(2,2′-bithiophene)} (P(NDI2OD-T2)), showing electron mobilities up to 1 $cm^2/V{\cdot}s$ in top-gate, bottom-contact organic field effect transistors (OFET). Since then, a large number of studies have been carried out to investigate the origin of the high electron mobility, paying specific attention to the relation between micro- and nanostructure, and charge transport properties.[26,27] While first investigations suggested P(NDI2OD-T2) films having a prevalent amorphous structure, grazing incidence X-ray scattering (GIXS) and atom force microscopy found a remarkable degree of molecular order in spin-coated films.[28−32] GIXS experiments provide evidence that the backbone adopts an unconventional face-on texture in the ordered phases with the $\pi-\pi$ stacking direction being orthogonal to the substrate and to the charge transport direction in OFET devices.[32] Using electron microscopy techniques, Takacs et al.[33] demonstrated that the polymer morphology is well ordered on the 10 nm scale and retains long-range correlation up to 1 μm. Recently, Luzio et al. demonstrated the effect of the film morphology on charge transport properties, showing that electron mobility can be tuned over 2 orders of magnitude by controlling the extent of oriented domains through the deposition process and the solvents used.[34] Furthermore, films with an edge-on morphology have been observed both after thermal treatment above the melting point (310 °C)[35] and in the case of Langmuir−Schäfer deposited multilayers.[36] Lemaur et al. have reported a computational study based on molecular dynamics calculations,

Received: November 15, 2014
Revised: January 6, 2015
Published: January 7, 2015

finding that in the crystalline domains P(NDI2OD-T2) chains show strong $\pi-\pi$ stacking between NDI2OD moieties, and tilted alkyl side chains for optimal packing.[37] Caddeo et al. performed an extended molecular dynamics and first-principles study, which investigated chain flexibility and structure of P(NDI2OD-T2) both in solution and in bulk film.[38]

Experimental techniques developed for the preparation of highly crystalline thin films have been constantly improved by exploiting different deposition methods.[39−43] Brinkmann et al.[44] have introduced different epitaxial crystallization techniques to grow polymer films characterized by a high crystallinity. By applying epitaxial crystallization to prepare thin films of P(NDI2OD-T2), highly oriented crystals with two different polymorphs can be obtained.[44] These two distinct polymorphs featured either segregated (form I) or mixed interchain stacks (form II) of naphthalene diimide and bithiophene. The structures have been identified through high-resolution transmission electron microscopy and electron diffraction.

Previously, we used a combination of vibrational spectroscopic techniques, IR absorption in double transmission geometry (IRA-TR), reflection absorption IR spectroscopy (RAIRS) at grazing incidence, and FT-Raman, together with density functional theory (DFT) calculations, as a powerful approach to investigate the intramolecular structure of P(NDI2OD-T2) chains and their orientation with respect to the substrate.[45] A first simple analytic model to correlate experimental IRA-TR/RAIRS intensities with structural parameters (e.g., the dihedral angle τ between NDI2OD and T2 units) has been suggested. We experimentally proved that NDI2OD and T2 units are not coplanar ($\tau \approx \pm 38°$). According to the structural model proposed, T2 units are found to lay flat and parallel to the substrate plane, while NDI2OD ones are tilted out of the surface. P(NDI2OD-T2) films obtained via spin coating resulted in morphologies far from the equilibrium conditions leading to the formation of thermodynamically unstable crystallites due to the complex interplay of solvent evaporation and molecular aggregation.[46−48]

The detailed intramolecular structure of the P(NDI2OD-T2) chains in both form I and form II crystalline films and the polymer chains orientation with respect to the substrate have not yet been experimentally solved.

To this end, we here propose the use of vibrational spectroscopy as a tool to investigate the molecular structure and chain orientation of the two different polymorphs in comparison to spin-coated film. Peculiar vibrational fingerprints of the spin-coated samples, hereafter referred to as scN2200, and of the two epitaxially grown films (form I and form II) have been found, which allow the determination of different preferential molecular orientations with respect to the substrate.

In particular, scN2200 and form I films feature mainly a face-on structure, with the polymer chain running parallel to the substrate. However, they show different orientations of the conjugated subunits, with the NDI2OD plane being tilted out of the substrate in the scN2200 case and nearly parallel to it in form I. In form II, however, polymer chains are tilted out of the surface. A quantitative interpretation of IRA-TR and RAIRS data is obtained through a new analytic model suitably developed for the description of both the orientations of the polymer chains and the structural units (i.e., NDI2OD and T2).

The approach here developed allows one to obtain insight into the architecture of organic conjugated polymers, and could be extended to a broad class of donor/acceptor polymers. For P(NDI2OD-T2), in particular, we obtained structural models for different films prepared through different techniques; these structures could be used as a starting guess for further structural refinements[49−51] and future charge transport investigations[50−52] based on molecular dynamics or ab initio calculations.

2. METHODS

2.1. Materials and Sample Preparation. *scN2200.* P(NDI2OD-T2) (see Scheme 1) purchased from the Polyera

Scheme 1. Structure Formula of P(NDI2OD-T2) Chemical Unit

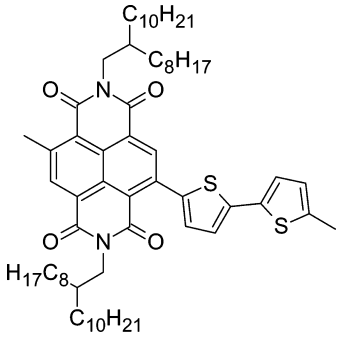

Corp. (ActivInk N2200) was used for the preparation of spin-coated films. The dispersity index (D) and the number-average molecular weight $M_{n,SEC}$ are ∼3 and 100 kg/mol, respectively. An aluminum mirror deposited on a square glass slide (of about 2 cm per side) was used as substrate both for IRA-TR microscopy and for RAIRS measurements. Each film was spin-coated from 10^{-3} M solution in *ortho*-dichlorobenzene (o-dcb) at 1000 rpm for 90 s and annealed to 80 °C for 90 s to facilitate solvent evaporation (film thickness in the range 10−20 nm). The spectra discussed in this Article are labeled as follows: N2200-IRA-TR (IRA-TR microscopy measurements) and N2200-Rairs (RAIRS experiments).

Epitaxially Grown Films. P(NDI2OD-T2) films of form I were prepared by slow directional epitaxial crystallization (DEC) using a published procedure.[40,44] In brief, first 400 mg of 1,3,5-trichlorobenzene (sublimed once for purification) and 2 mg of P(NDI2OD-T2) (M_n = 31 kg/mol, M_w = 123 kg/mol, D = 3.97) were heated to 65 °C until melting of TCB. After being cooled to room temperature, a uniform powder of TCB/P(NDI2OD-T2) blend was obtained. Twenty-five milligrams of this powder was placed on an ITO or gold-coated glass substrate. It was covered by a second glass slide coated with an oriented poly(tetrafluoroethylene) substrate (PTFE) (prepared by friction transfer[40] to guide the growth of TCB). This was heated on a hot stage until melting and uniform spreading of the TCB/P(NDI2OD-T2) solution between the PTFE-coated glass slide and the second ITO or gold-coated glass substrate. This system was moved slowly in a temperature gradient at 20 μm/s to induce DEC of P(NDI2OD-T2). The sample was then placed in a vacuum to evaporate TCB. Highly oriented P(NDI2OD-T2) films were recovered, and suitable areas were selected by optical microscopy on a Leica DMR-X. As expected from our previous work, DEC generates form I P(NDI2OD-T2) films. To obtain the form II films, samples of form I were placed in a linkam LTS420 hot stage and annealed at 300 °C for 1 min and slowly cooled (0.5 °C/min) to room temperature. Transmission electron microscopy was performed with a Philips CM 12 (120 keV) microscope equipped with a

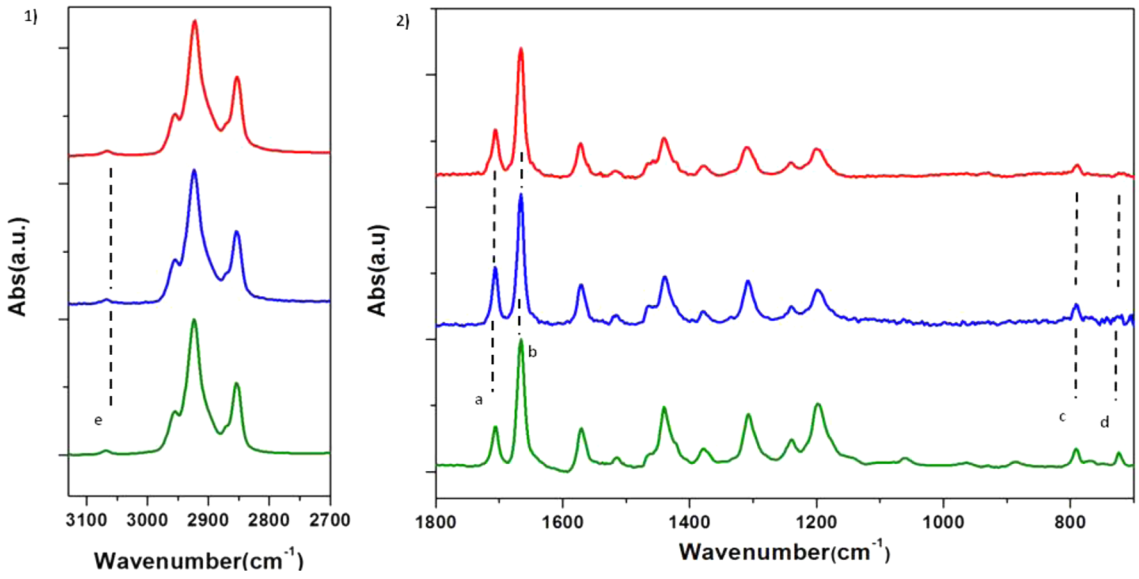

Figure 1. Micro-FTIR spectra of scN2200 (green spectrum), form I (blue spectrum), and form II (red spectrum) samples. Panel 1: 3100−2700 cm^{-1} spectral region. Panel 2: 1800−700 cm^{-1} spectral region. The intensity scale in panel 1 is normalized to the 2920 cm^{-1} band, and in panel 2 to the 1666 cm^{-1} (band b).

CCD MVIII digital camera. The image treatments were carried out using AnalySYS (Soft Imaging Systems) and ITEM (FEI) software.

Glass substrates covered with 80 nm gold were used for RAIRS and IRA-TR microscopy experiments. The spectra obtained will be referred to as follows: form I-IRA-TR and form II-IRA-TR for IRA-TR microscopy experiments, and form I-RAIRS and form II-RAIRS for grazing angle RAIRS measurements.

Vibrational Spectra. IRA-TR spectra were recorded (256 scans at 4 cm^{-1} resolution) with an FTIR Nicolet Nexus spectrometer coupled to a Continuμm FTIR microscope on samples at room temperature in double transmission mode. RAIRS measurements were carried out by means of a Spectra Tech Inc. FT-80 grazing-angle accessory (82° reflection angle, 4 cm^{-1} resolution, and 256 scans) at room temperature. The accessory contains a gold wire grid polarizer, which ensures that only p-polarized IR light reached the detector. Spectra treatment and measurement of bands intensities were carried out by OMNIC software. The spectroscopic data discussed in this Article and used for the determination of the polymer orientation correspond to the samples illustrated above, which have been selected as the most representative of three different sets of samples, scN2200 and films of form I and form II. To gather information on the reproducibility of the data and to judge on the experimental uncertainty, the data analyzed were compared to experiments on different samples and from different spectra taken from the same samples.

3. RESULTS AND DISCUSSION

3.1. FTIR Spectra and Band Assignments of P(NDI2OD-T2) Films: scN2200, Form I, and Form II Films. Figure 1 shows Micro-IRA-TR spectra of the two epitaxial films, form I (blue line) and form II (red line), and of scN2200 film (green). No differences in terms of band shape and frequencies are present among the spectra, indicating that the main vibrational modes are not perturbed by the sample morphology.[45]

Five principal bands can be identified as markers of the polymer structure (see Scheme 1): a (1706 cm^{-1}) and b (1666 cm^{-1}) bands, corresponding to the C═O symmetric and antisymmetric stretching, respectively, c (790 cm^{-1}) band, corresponding to the CH out-of-plane (OPLA) mode of the T2 unit, d (723 cm^{-1}) band, corresponding to the CS stretching, and the weak band e (3072 cm^{-1}) band, assigned to the CH bonds stretching belonging to the T2 unit.

The transition dipole moment associated with these bands features different polarizations: band a is polarized in the direction of the long NDI2OD symmetry axis and band b along the short one; that is, they are mainly orthogonal and parallel to the polymer chain, respectively; band c shows a polarization perpendicular to the thiophene rings (i.e., T2 local plane); while the d and e bands are polarized in the T2 plane. The intensity of these bands in the three different films is important to discuss the orientations of the polymer chains and the conjugated units relative to the substrate.[45]

A non-negligible difference can be found considering the intensities of bands a and b, once normalized with respect to the whole CH stretching region (3200−2800 cm^{-1}).[53] Form II and scN2200 have similar intensity values, $I^{(a+b)}/I^{CH}$ (form II) = 0.16 and $I^{(a+b)}/I^{CH}$ (scN2200) = 0.15, respectively, whereas form I has $I^{(a+b)}/I^{CH}$ = 0.18. These values should be compared to the same ratio as obtained for N2200 in solution: $I^{(a+b)}/I^{CH}$ = 0.54. The latter is different from those measured in the films, suggesting that a non-negligible orientational order is present in solid-state samples. In particular, because bands a and b correspond to normal modes localized on the NDI2OD unit, the change of their IR intensities can be ascribed to the occurrence of a preferential orientation of the NDI2OD units with respect to the substrate. When the material is no longer isotropic, the three Cartesian directions are no more equivalent, and vibrational transitions with oscillating dipoles oriented in the propagating direction of the IR beam cannot be excited and observed. In the case of IR transmission experiments at normal incidence, this happens for those vibrational modes polarized in the direction orthogonal to the sample surface. Accordingly, we can infer that the change of $I^{(a+b)}/I^{CH}$ from form II or scN2200

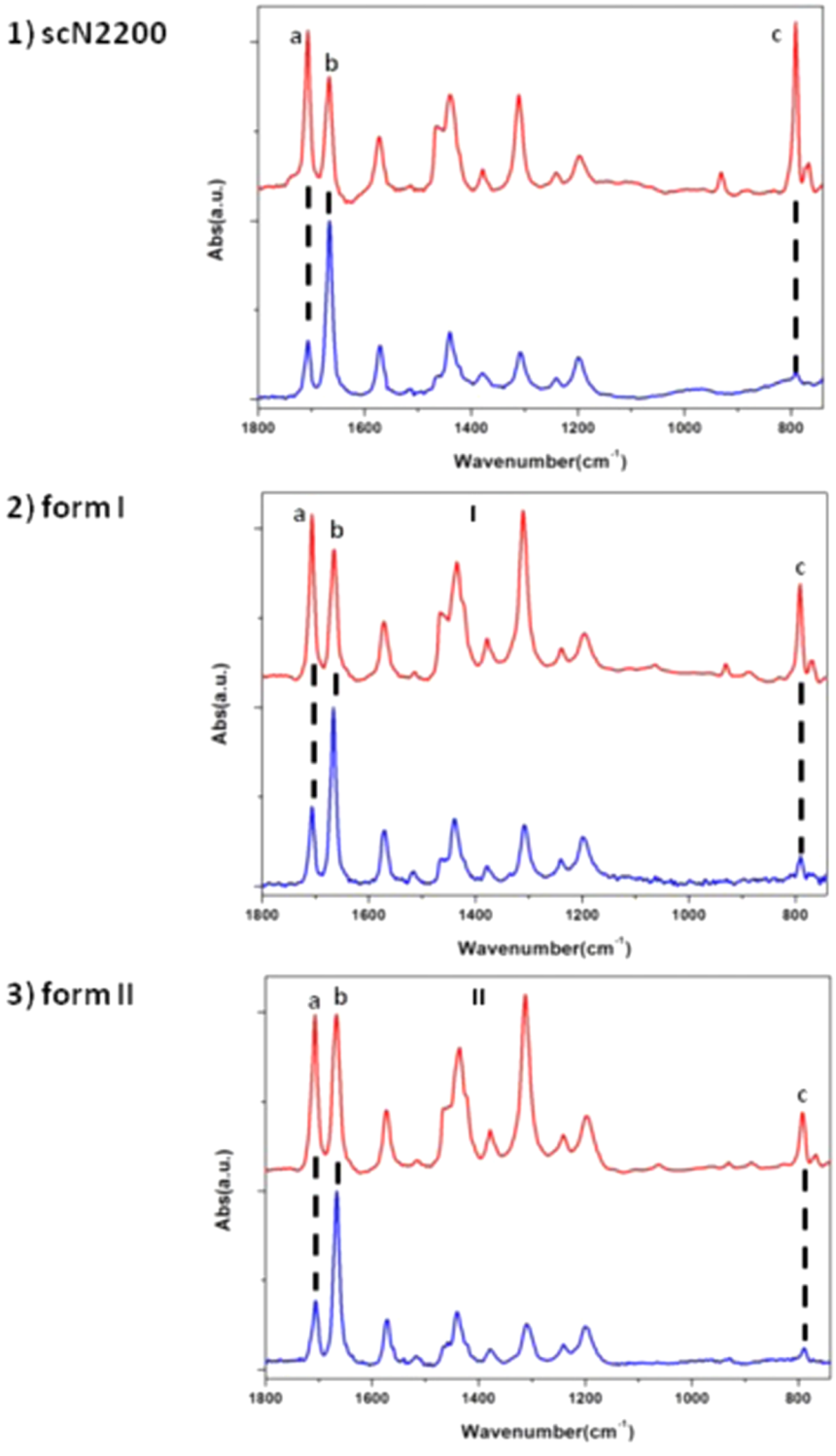

Figure 2. Comparison between RAIRS (red spectra) and IRA-TR (blue spectra) in the 1800−700 cm^{-1} spectral region. Panel 1: scN2200. Panel 2: form I. Panel 3: form II. The marker bands are labeled according to the manuscript notation.

to form I can be taken as evidence of a different orientation of the NDI2OD units occurring in the latter. In particular, because IR experiments are carried out at normal incidence with respect to the substrate, in form I the local plane defined by the NDI2OD unit lies more parallel to the substrate plane.

3.2. RAIRS versus IR Transmission Spectra of Spin-Coated and Epitaxially Grown Films. To better investigate the molecular structure and the polymer chain arrangements in the different samples, we compared IRA-TR spectra with RAIRS measurements (Figure 2). In RAIRS a very thin layer (10−20 nm) of the polymer is deposited on a high reflective metallic substrate; the angle of incidence (and reflection) of the IR beam is between 75° and 85°. This experimental setup guarantees that the s-component (perpendicular to the incidence plane) of the electric field, of both incident and reflected beams, is canceled at the metal surface; instead, the p-component (polarized in the incidence plane) of both the incident and the reflected beams additively produces a strong

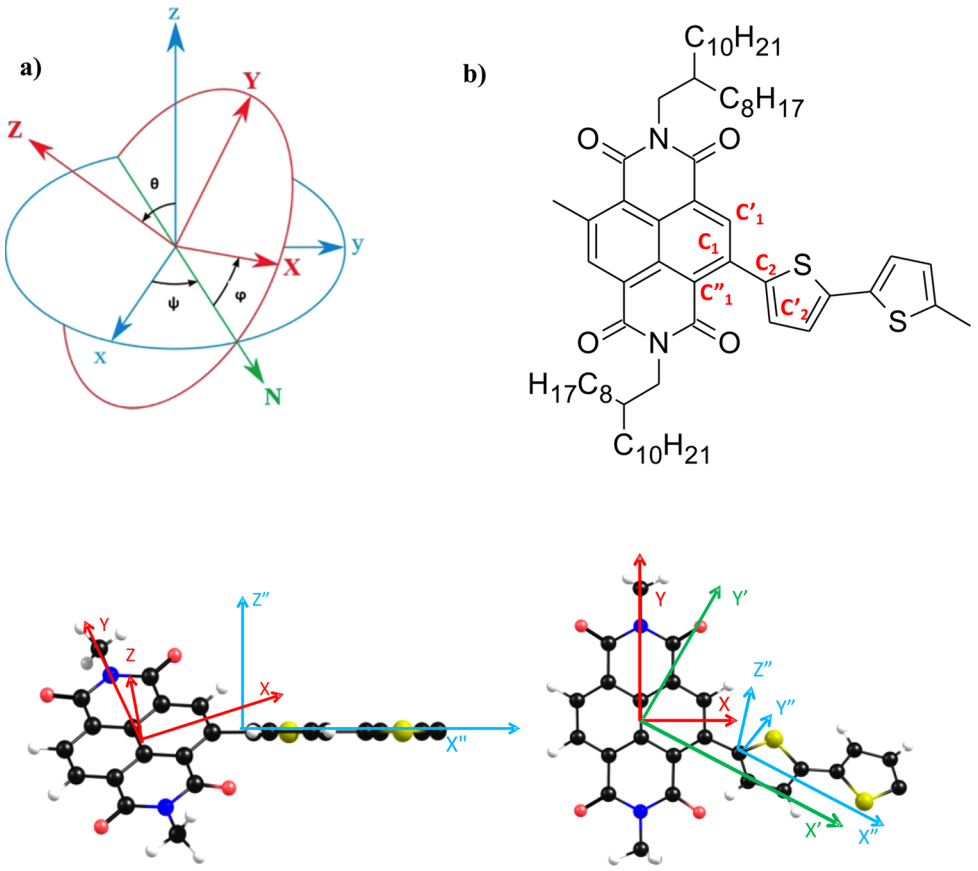

Figure 3. (a) Laboratory Cartesian reference system (x, y, z) and local symmetry adapted NDI2OD system (X, Y, Z), with definition of the Euler angles. Sketches of the copolymer unit: (b) chemical structure showing the atomic labels adopted to define τ and α and (bottom) two different views of the equilibrium conformation (*anti* conformation, $\tau = 42°$). Local reference systems: red = symmetry adapted system NDI2OD (X, Y, Z), green = rotated local reference system (X', Y', Z') of NDI2OD, and light blue = local reference system (X'', Y'', Z'') of T2 unit.

electric field, directed perpendicular to the metal surface. Therefore, the p-polarized beam at grazing angle can be strongly absorbed by a transition moment oriented perpendicular to the film surface.[52] Normal modes (Q_k) mainly polarized perpendicular to the substrate ($\partial M^z/\partial Q_k \neq 0$, z orthogonal to the substrate) are RAIRS active, while normal modes polarized in the substrate plane ($\partial M^x/\partial Q_k \neq 0$ and/or $\partial M^y/\partial Q_k \neq 0$) are RAIRS inactive.[54]

IRA-TR measurements are complementary to RAIRS because in the normal incidence the electric field vector oscillates in the surface plane, so that only transitions showing a nonvanishing projection of $\partial\mathbf{M}/\partial Q_k$ in the (x, y) plane are observed.

With respect to the IR spectrum recorded in transmission, the RAIRS spectrum of the scN2200 (Figure 2, panel 1) shows an enhancement of the c and a bands intensities and a decrease of those of the b and d bands. This spectral change has been discussed by Giussani et al.,[45] showing that the polymer chains lie preferentially parallel to the substrate surface according to a face-on arrangement, with T2 units being flat to the substrate surface and NDI2ODs tilted with an angle of about 38° (experimental determination).

Comparing the IR transmission and RAIRS spectra of form I and form II, we can observe that the RAIRS spectrum of form I shows an increase of band b and a decrease of band c with respect to scN2200, and that the same changes are even more marked in form II, especially for band c. This trend confirms that the two polymorphs present a different molecular orientation with respect to the substrate. The increase of band b in RAIRS (polarized mainly parallel to the polymer chain) indicates that the chains are no longer parallel to the surface, whereas the decrease of band c suggests that the T2 units are no longer coplanar to the substrate.

To rationalize these spectroscopic features, we developed a new analytic model able to provide expressions for the components of the dipole moment derivative vectors ($\partial\mathbf{M}/\partial Q_k$) associated with the normal modes (Q_k) as a function of suitable geometric parameters describing the orientation of the two units (NDI2OD and T2) with respect to the laboratory reference system (x,y,z).

In such a way, the model correlates experimental IR and RAIRS intensities to (1) structural parameters, as the intramolecular torsional angle τ between NDI2OD and T2 units and the angle α, related to a $C_1'C_1C_2$ valence angle (see Figure 3), and (2) orientations of NDI2OD and T2 units with respect to the substrate, through the definition of the Euler angles (see below and Figure 3).

From the comparison of the IRA-TR and RAIRS spectra (Figure 2), it is concluded that T2 units in form I and form II are not parallel with respect to the substrate. For this reason, we have to consider extra degrees of freedom to take into account the orientations of both T2 and NDI2OD units. The orientation of NDI2OD units will determine the relative intensities of bands a and b, while the intensity behavior of band c is related to the orientation of T2 unit. However, once the orientation of NDI2OD unit is defined through the

Table 1. Analytic Expressions for IR Intensities (Bands a and b) and for the Intensities Ratio $R^{b/a}$ ($R^{b/a} = I^b/I^a$) As Obtained with Different Experimental Setups (for Films)[a]

	band a	band b
IR transmission	$I_a^{TR} \propto \lvert\partial\mathbf{M}/\partial Q_a\rvert^2(\sin^2\varphi + \cos^2\varphi\cdot\cos^2\theta)$	$I_b^{TR} \propto \lvert\partial\mathbf{M}/\partial Q_b\rvert^2(\cos^2\varphi + \sin^2\varphi\cdot\cos^2\theta)$
RAIRS	$I_a^{RAIRS} \propto \lvert\partial\mathbf{M}/\partial Q_a\rvert^2(\cos^2\varphi\cdot\sin^2\theta)$	$I_b^{RAIRS} \propto \lvert\partial\mathbf{M}/\partial Q_b\rvert^2\ (\sin^2\varphi\cdot\sin^2\theta)$
solution	$I_a^{SOL} \propto \lvert\partial\mathbf{M}/\partial Q_a\rvert^2$	$I_b^{SOL} \propto \lvert\partial\mathbf{M}/\partial Q_b\rvert^2$
	analytic expressions for intensities ratios (I^b/I^a)	
$R_{TR}^{b/a}$	$(\lvert\partial\mathbf{M}/\partial Q_b\rvert^2/\lvert\partial\mathbf{M}/\partial Q_a\rvert^2)(\cos^2\varphi + \sin^2\varphi\cdot\cos^2\theta)/(\sin^2\varphi + \cos^2\varphi\cdot\cos^2\theta)$	
$R_{RAIRS}^{b/a}$	$(\lvert\partial\mathbf{M}/\partial Q_b\rvert^2/\lvert\partial\mathbf{M}/\partial Q_a\rvert^2)tg^2\varphi$	
$R_{SOL}^{b/a}$	$(\lvert\partial\mathbf{M}/\partial Q_b\rvert^2/\lvert\partial\mathbf{M}/\partial Q_a\rvert^2)$	

[a]See details in Supporting Information S1. The Euler angle θ varies in the range $[-\pi/2, \pi/2]$ and the angle φ in the range $[-\pi, \pi]$.

Table 2. Analytic Expressions for IR Intensities (Band c) and for Intensities Ratio $R^{c/b}$ ($R^{c/b} = I^c/I^b$) Obtained from Different Experiments (for Film)[a]

	band c
IR transmission	$I_c^{TR} \propto \lvert\partial M^{Z''}/\partial Q_c\rvert^2\{\{\cos\tau\cdot\sin\theta - \sin\tau\cdot\cos\theta\cdot\cos(\alpha-\varphi)\}^2 + \sin^2\tau\cdot(\sin^2(\alpha-\varphi))\}$
RAIRS	$I_c^{RAIRS} \propto \lvert\partial M^{Z''}/\partial Q_c\rvert^2\{\cos\tau\cdot\cos\theta + \sin\tau\cdot\sin\theta\cdot\cos(\alpha-\varphi)\}^2$
	analytic expressions for the intensities ratio (I^c/I^b)
$R_{TR}^{c/b}$	$(\lvert\partial\mathbf{M}/\partial Q_c\rvert^2/\lvert\partial\mathbf{M}/\partial Q_b\rvert^2)\{\{\cos\tau\cdot\sin\theta - \sin\tau\cdot\cos\theta\cdot\cos(\alpha-\varphi)\}^2 + \sin^2\tau\cdot(\sin^2(\alpha-\varphi))\}/(\cos^2\varphi + \sin^2\varphi\cdot\cos^2\theta)$
$R_{RAIRS}^{c/b}$	$(\lvert\partial\mathbf{M}/\partial Q_c\rvert^2/\lvert\partial\mathbf{M}/\partial Q_b\rvert^2)\{\cos\tau\cdot\cos\theta + \sin\tau\cdot\sin\theta\cdot\cos(\alpha-\varphi)\}^2/(\sin^2\varphi\cdot\sin^2\theta)$
$R_{TR}^{c/b}/R_{RAIRS}^{c/b}$	$\{\{[\cos\tau\cdot\sin\theta - \sin\tau\cdot\cos\theta\cdot\cos(\alpha-\varphi)]^2 + \sin^2\tau\cdot(\sin^2(\alpha-\varphi))\}(\sin^2\varphi\cdot\sin^2\theta)\}/\{(\cos^2\varphi + \sin^2\varphi\cdot\cos^2\theta)[\cos\tau\cdot\cos\theta + \sin\tau\cdot\sin\theta\cdot\cos(\alpha-\varphi)]^2\}$

[a]See details in Supporting Information S2.

definition of suitable Euler angles (see Supporting Information, Figure S1.1), the orientation of T2 can be described considering the value of the torsional angle τ.

3.3. Analytic Model Connecting IRA-TR/RAIRS Intensities to Structural Parameters. The model here proposed requires the introduction of four different Cartesian coordinates systems, as illustrated in Figure 3 (see also the Supporting Information for a detailed description of the conventions adopted):

(i) (x, y, z) is the substrate or laboratory reference Cartesian system, with (x, y) in the substrate plane and z normal to it;
(ii) (X, Y, Z) is the first local system with Z axis orthogonal to the plane defined by the condensed naphthalene rings; X and Y axes are defined according to the local D_{2h} symmetry of the NDI2OD unit; that is, (X, Y, Z) is a symmetry adapted local system;
(iii) (X', Y', Z') is the second local system obtained by rotating system (ii) around the Z axis to get X' parallel to the C_1C_2 bond;
(iv) (X'', Y'', Z'') is the third local system where (X'', Y'') defines the plane that contains the T2 unit (assumed to be fully planar for the sake of simplicity). X'' coincides with X'.

The analytical expression obtained for the intensity ratios of the marker bands are reported in Tables 1 and 2. They connect the spectroscopic parameters $\partial\mathbf{M}/\partial Q_k$ to four variables, two structural (α and τ) and two orientational, which define the rotation between the NDI2OD symmetry adapted local system (X, Y, Z) and the laboratory system (x, y, z), the angle θ between z and Z axes and the angle φ between X axis and the nodes axis N (see Supporting Information S1).

The expressions in Tables 1 and 2 hold within the following hypothesis:

(i) the orientation of the polymer units with respect to the z axis of the substrate system is ideal and the material is considered to be isotropic in the (x, y) plane. NDI2OD units are characterized by the same Euler angles (θ, φ), while ψ is arbitrarily chosen by each chain.
(ii) The angle connecting the symmetry adapted local system (X, Y, Z) to the second system (X', Y', Z') is defined by the intramolecular parameter α, namely by the angle between the C_1-C_2 direction and the local horizontal axis X. The angle between Y' and Y'' (and Z' and Z'') is defined by the intramolecular parameter τ, the torsional angle around the C_1-C_2 bond. τ corresponds to the dihedral angle between the two planes (X'', Y'') and (X', Y'), containing T2 and NDI2OD (see the Supporting Information for definition).

In addition, the following relationships have to be considered:

(a) the RAIRS intensity of a given normal mode is defined by the z component of the transition dipole moment: $I_k^{RAIRS} \propto \lvert\partial M^z/\partial Q_k\rvert^2$;
(b) the IRA-TR intensity of Q_k mode is $I_k^{TR} \propto \lvert\partial M^x/\partial Q_k\rvert^2 + \lvert\partial M^y/\partial Q_k\rvert^2$;
(c) the IRA-TR intensity of Q_k mode in an isotropic sample (solution) is $I_k^{SOL} \propto \lvert\partial\mathbf{M}/\partial Q_k\rvert^2 = \lvert\partial M^x/\partial Q_k\rvert^2 + \lvert\partial M^y/\partial Q_k\rvert^2 + \lvert\partial M^z/\partial Q_k\rvert^2$.

According to the above points, the equations in Tables 1 and 2 refer to an individual polymer structural unit (NDI2OD-T2). To describe the full polymer simply referring to one structural unit, the occurrence of a regular conformation of the chain has to be considered, allowing the same set (ψ, θ, φ) of Euler angles for all of the NDI2OD units belonging to the chain.

Regular and stable polymer structures (reported in Supporting Information Figure S.3) can be obtained if each torsional angle along the chain can assume one of the four values $\pm 42°$, $\pm 138°$.[55] In such a way, the conformation of the whole chain is described by the sequence (...,(τ, $\bar{\tau}$), (τ, $\bar{\tau}$), (τ, $\bar{\tau}$),...), with τ the internal dihedral angle and $\bar{\tau}$ the external one, connecting two repeat units.

We can obtain structures characterized by translational symmetry between adjacent structural units (extended chains),

Table 3. Comparison between Theoretical and Experimental Values of $R_{TR}^{b/a}$, $R_{RAIRS}^{b/a}$, $R_{TR}^{c/b}$, $R_{RAIRS}^{c/b}$, and $R_{TR}^{c/a}$, $R_{RAIRS}^{c/a}$ for scN2200, Form I, and Form II[a]

φ	θ	$R_{RAIRS}^{b/a}$	$R_{TR}^{b/a}$	$R_{RAIRS}^{c/b}$	$R_{RAIRS}^{c/a}$	$R_{TR}^{c/b}$	$R_{TR}^{c/a}$	$R_{TR}^{c/b}/R_{RAIRS}^{c/b}$
				scN2200				
29.25	**40.16**	**0.94**	**3.95**	**1.21**	**1.14**	**0.00**	**0.00**	**0.00**
−29.25	−40.16	0.94	3.95	0.15	0.14	0.12	0.46	0.80
29.25	−40.16	0.94	3.95	0.02	0.02	0.13	0.52	5.81
−29.25	40.16	0.94	3.95	0.75	0.71	0.05	0.20	0.07
	exp.	**0.94**	**3.95**	**1.02**	**0.96**	**0.03**	**0.13**	**0.03**
				form I				
28.62	20	0.89	3.21	3.84	3.43	0.02	0.06	0.00
−28.62	−20	0.89	3.21	1.50	1.34	0.08	0.26	0.05
28.62	**−20**	**0.89**	**3.21**	**0.99**	**0.88**	**0.10**	**0.31**	**0.10**
−28.62	20	0.89	3.21	2.99	2.67	0.04	0.13	0.01
	exp.	**0.89**	**2.66**	**0.52**	**0.53**	**0.09**	**0.25**	**0.18**
				form II				
32.14	46.40	1.18	4.09	0.80	0.95	0.00	0.00	0.00
−32.14	−46.40	1.18	4.09	0.07	0.08	0.13	0.53	1.96
32.14	−46.40	1.18	4.09	0.00	0.00	0.14	0.58	218.06
−32.14	**46.40**	**1.18**	**4.09**	**0.44**	**0.52**	**0.06**	**0.26**	**0.14**
	exp.	**1.18**	**4.08**	**0.28**	**0.34**	**0.04**	**0.15**	**0.13**

[a]The bold characters highlight the best choice of parameters to reproduce the experimental ratio, as reported in the last row of each section.

or chains characterized by helical symmetry (see Supporting Information Figure S.3). The first one corresponds to the choice $\overline{\tau} = -\tau$. The second ones refer to structures with $\overline{\tau} = \tau$ resulting in a different orientation of the local planes of the subsequent NDI2OD units (and T2 units).

Our model assumes that each individual structural unit should be characterized by the same orientation with respect to the substrate, and for this reason helix structures do not fit our choices. According to the selected value of τ, we can obtain *anti* or *syn* chains; moreover, a systematic inversion of the signs of the pair $(\tau, \overline{\tau})$ gives rise to mirror symmetry related structures (see Supporting Information Figure S.3). Considering that effective chain packing is expected for straight chains, we can argue that our models (with $\overline{\tau} = -\tau$, i.e., translational symmetry) are the most suitable for describing the crystalline domains of form I and form II films.

However, regular conformations cannot be considered fully realistic for describing amorphous phases (as those present in spin-coated films), characterized by conformational disorder. In this regard, it should be noticed that the two different pairs of torsional angles, $\tau = 42°$, $\tau = -138°$ and $\tau = -42°$, $\tau = 138°$, lead to the same expression for IRA-TR and RAIRS intensities (Table 2), because they keep the same orientation of the local planes (compare, for instance, Supporting Information Figure S.3.a1 and a4). This property guarantees that the equations reported in Tables 1 and 2 hold also for the description of chains containing some conformational disorder.

The absolute values of $|\varphi|$ and $|\theta|$ can be directly derived from the intensity ratios of b and a bands in RAIRS and transmission experiments, provided that the ratio $(|\partial\mathbf{M}/\partial Q_b|^2/|\partial\mathbf{M}/\partial Q_a|^2)$ is obtained by the IR spectrum in solution. Once φ and θ are known, it is possible to obtain α and τ as well, which determine the orientation of T2 units with respect to NDI2OD. However, the determination of the structural parameters α and τ would require the knowledge of the signs of φ and θ, which define the molecular orientation. According to our model (see the Supporting Information), the sign of φ determines the arrangement of the polymer backbone with respect to the substrate: a positive value of φ, and close to α, corresponds to a polymer chain mostly lying parallel to the substrate. A negative value of φ indicates, however, a polymer chain tilted out of the substrate plane. θ rules instead the tilting of the NDI2OD plane with respect to the substrate.

We can get insight into the signs of φ and θ considering structural parameters α and τ obtained by DFT calculations. In this way, the expressions of Table 2 can be exploited for a prediction of intensities ratios between c and b bands, according to different choices of the signs for φ and θ. A direct comparison of the experimental intensity ratios $R_{TR}^{c,b}$ and $R_{RAIRS}^{c,b}$ with the predicted values will allow one to critically analyze the different choices of sign for φ and θ.

3.4. Analysis of the Copolymer Structure and Orientation. Starting from the experimental values obtained for $|\varphi|$ and $|\theta|$, and considering all of the possible combinations of $\pm\varphi$ and $\pm\theta$ pairs, eight different sets of geometrical parameters, α, φ, τ, θ, are given. However, because a change of sign for τ has the same effect of changing the sign of θ (see equations in Table 2), the whole set of theoretically predicted intensity ratios can be obtained considering four sets of parameters $((\alpha, \varphi, \tau, \theta)$ and $(\alpha, \varphi, -\tau, -\theta)$ are equally acceptable). In Table 3, for each P(NDI2OD-T2) sample (scN2200, form I, form II), it is possible to make the best choice of (φ, θ) values, based on the best agreement with the intensity ratio experimentally determined.

From Table 3 it results that $|\varphi|$ is close to 30° for the three films. Because the function $tg^2\varphi$ (see Table 1) is rather steep around 30°, changes of φ bring non-negligible changes of $R_{RAIRS}^{b/a}$: this trend explains why the observed modulation of $R_{RAIRS}^{b/a}$ gives rise to very small variations of $|\varphi|$.

For scN2200 and form II, $|\theta|$ is about 40°, which is close to the τ value obtained from DFT calculations. Unfortunately, in the case of form I, we cannot extract an estimate of $|\theta|$ directly from the experimental value of $R_{TR}^{b/a}$ ($R_{TR}^{b/a} = 2.66$). Indeed, in the range of φ values $0 < \varphi < 45°$, the theoretical expression for $R_{TR}^{b/a}$ does not admit a solution for $R_{TR}^{b/a} < 3$. The limit value $R_{TR}^{b/a} = 3$ coincides with the experimental $R^{b/a}$ value characteristic of the solution, that is, for an isotropic sample, but it would be

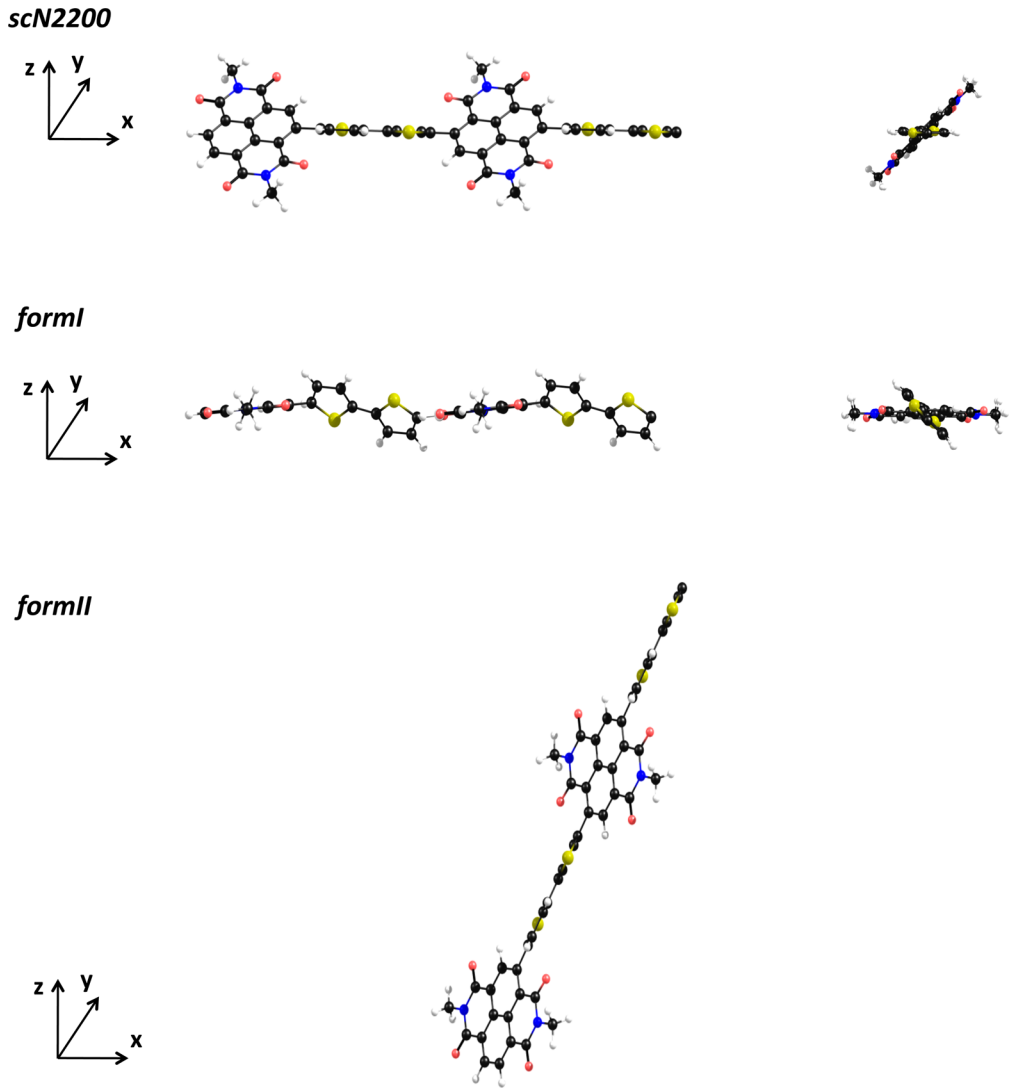

Figure 4. Models of P(NDI2OD-T2) chains with regular conformation (τ = 42°, τ = −42°) showing different orientations with respect to the substrate surface (x, y, z Cartesian coordinate system).

obtained also in the case of a polymer orientation, showing NDIO2D units perfectly parallel to the substrate.

The experimental result $R_{TR}^{b/a}$ = 2.66 can be taken as the evidence of a structure characterized by a nearly perfect face-on arrangement of the NDIO2D units (θ close to 0°). To give a quantitative estimate of θ, we explored a range of $|\theta|$ (from 0° to 30°) and established the best choice based on the match with the whole set of experimental data. The best set of predicted intensities is obtained for θ = −20°.

By comparing the theoretical values in Table 3 with the experimental ones, we can draw the following conclusions.

Regarding the scN2200 sample, positive values of φ and θ, being $\varphi \cong \alpha$ and $\theta \cong \tau$, are the best choice (see Figure 4, model A). These findings are in agreement with ref 45 and indicate a polymer backbone that lies preferentially parallel to the substrate surface in the so-called face-on arrangement, with T2 units flat and NDI2OD units tilted with an angle of ∼40°.

An alternative choice with a negative φ and a positive θ value would nicely fit the experimental data ($R_{TR}^{c/b}/R_{RAIRS}^{c/b}$: 0.07 (theo) vs 0.03 (exp)). This choice, however, would suggest a polymer arrangement with the chain axis out of the substrate plane (φ < 0). To discriminate between the two different solutions, other spectral features have to be considered, as the intensity of band e (CH stretching of the T2 unit). Band e, which is polarized in the T2 local plane, shows negligible RAIRS intensity but is strong in the IR transmission spectrum.[45] This behavior is compatible with a face-on arrangement, featuring T2 units lying parallel to the substrate.

For form I the best solution corresponds to a positive value of φ and a negative value of θ, the absolute values of which are remarkably lower than those for scN2200. θ determines to what extent the NDI2OD units are tilted with respect to the substrate, and θ = −20° suggests that in form I the NDI2OD units are nearly flat on the substrate, and consequently the T2 units are tilted out of the surface plane (see Figure 4, model B).

This is in agreement with the spectroscopic evidence showing a decrease of band c and an increase of band b in the RAIRS spectrum (Figure 2). On the other hand, the positive value of φ indicates that also in form I the backbone is preferentially parallel to the substrate surface in the so-called face-on arrangement.

Going from scN2200 to form I, a rotation of the polymer chain around its axis occurs in a way that NDI2OD units are

nearly parallel to the substrate while T2 units are tilted (see Figure 4).

For form II, the best agreement is obtained for negative φ and positive θ values, the latter being similar to that of scN2200. These findings indicate that in form II the P(NDI2OD-T2) backbone is tilted out of the substrate with an angle $\delta = \alpha - \varphi$ of about 60°, showing a chain orientation never observed in the previous studies (see Figure 4, model C).

This polymer orientation leads to an increase of band b and to a remarkable decrease of band c in the RAIRS spectrum (see Figure 2).

3.5. Transmission Electron Microscopy Results. TEM data were collected to get insight on the crystalline structure of form I and form II, and to support the RAIRS data and validate the structural analysis.

TEM brightfield (BF) and electron diffraction (ED) patterns of the P(NDI2OD-T2) films (Figure 5) confirm the presence

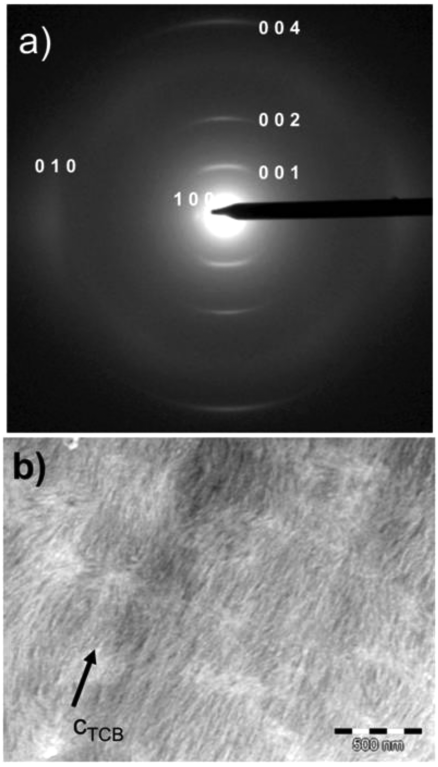

Figure 5. Electron diffraction pattern (a) and film morphology (b) of an oriented P(NDI2OD-T2) film of form I prepared by slow directional epitaxial crystallization in TCB.

of the form I of this polymer in the oriented films. As seen in the BF image, the fibrillar morphology of the films is observed with the fibrils oriented along the c_{TCB} axis of the substrate used for epitaxy. The ED pattern shows mainly strong (00*l*) reflections with a dominant and broad (001) peak. The large azimuthal spread of this peak is related to the monoclinic character of the unit cell of form I as seen clearly in rubbed P(NDI2OD-T2) films of form I.[44] Along the equator of the ED pattern, both weak (100) and broad (010) reflections are observed, indicative of a fiber symmetry of the sample (not a single contact plane of form I domains on the substrate).

Transformation to form II upon annealing at 300 °C is confirmed by the ED pattern (Figure 6), which shows a much weaker (001) reflection with an intensity below that of (002), that is, the fingerprint of form II.[44]

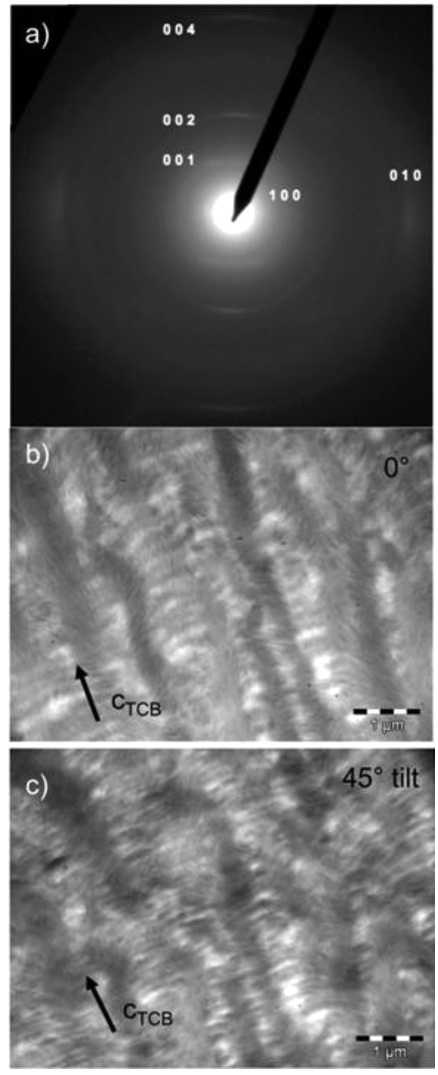

Figure 6. Electron diffraction pattern (a) and film morphology (b and c) of an oriented P(NDI2OD-T2) film of form II obtained by thermal annealing at 300 °C of form I. The tilting axis is perpendicular to c_{TCB}.

It is worth stressing that given the larger MW of the sample used for the preparation of the oriented films here (M_n = 31 kg/mol, M_w = 123 kg/mol, $Đ$ = 3.97) as compared to a previous study on a sample with M_n = 22 kg/mol, M_w = 83 kg/mol, $Đ$= 3.82,[44] the overall ED patterns show only a few reflections, and mixed reflections are missing. Whereas in the previous study regular lamellar domains of form II were evidenced for the lower MW sample with M_n = 22 kg/mol, the situation is somewhat different for the polymer used in this study.

Figure 6 shows the BF image of the films when the incident e-beam is oriented perpendicular to the film plane and after tilting the sample around an axis perpendicular to the c_{TCB} direction (chain axis direction). The morphology in the nontilted samples shows a reminiscence of the fibrillar structure observed in form I films as well as some contrast modulation with a 150−200 nm period that reminds of a lamellar morphology. It is however clearly distinct from the neat

lamellar morphology observed in our previous studies for lower-MW P(NDI2OD-T2).[44,49]

Interestingly, after a 40−50° tilt of the sample around $c_{p(NDI2OD-T2)}$, this lamellar structure becomes more obvious, which may indicate that the lamellae are tilted with respect to the substrate plane; that is, the chain axis direction may not strictly lie in the plane of the substrate.

This feature further supports the RAIRS data and the structural analysis reported, confirming that P(NDI2OD-T2) assumes, in high MW samples, a chain orientation for form II, which is no longer parallel to the substrate but tilted.

Overall, the results obtained by TEM on these form II films suggest that both MW and dispersity control very strongly the morphology of P(NDI2OD-T2) in thin oriented films. Annealing at 300 °C seems not sufficient to generate a regular lamellar morphology of form II for such high M_w samples. It is possible that chain entanglements in high-MW P(NDI2OD-T2) impede efficient reorganization of the films during thermal annealing to form a regular lamellar structure. It must also be stressed that pure form II films were initially obtained on oriented PTFE substrates, which was thought to ease alignment and heterogeneous nucleation of p(NDI2OD-T2) form II domains.[44]

4. CONCLUSIONS

P(NDI2OD-T2), an efficient n-type polymer semiconductor, has been investigated through vibrational spectroscopy in spin-coated and epitaxially grown films (named form I and form II).

For the first time, an analytic model connecting the IR parameters (i.e., $\partial \mathbf{M}/\partial Q_k$) to structural variables has been proposed to rationalize the structure and orientation of the polymer chains in the three different films.

Four geometrical variables are adequate to characterize the polymer: two intramolecular parameters, the dihedral angle τ and the bond angle α, and two orientational parameters, the Euler angles φ and θ describing the NDI2OD orientation with respect to the substrate.

Spin-coated films and form I samples are both characterized by a face-on arrangement of the chains; however, they show a different orientation of NDI2OD and T2 local planes. Spin-coated films present T2 units flat on the substrate and NDI2OD units tilted by ∼42°, while form I shows NDI2OD units mostly parallel to the substrate (∼20°) and T2 units tilted out.

The most thermodynamically stable form II presents, for high molecular weight samples, a completely different arrangement of the chains, with the polymer chain axis pointing out of the substrate plane.

The simple model connects vibrational observables to structural parameters, and it is suitable to characterize highly crystalline organic materials, such as those obtained via epitaxial growing methods.

On the other hand, the occurrence of chain orientation does not necessarily imply the existence of large, highly ordered 3D crystalline domains in P(NDI2OD-T2) films, which are weakly present in the case of spin-coated samples. However, according to our results, one can conclude that also in this last case a remarkable supramolecular order, in terms of chain orientation, is present. Moreover, our analysis suggests that polymer chains are mainly straight, a property that implies a high conformational order, nregular conformations of the chains also in the amorphous phase.

This conclusion agrees with the description reported by Luzio et al.,[34] in which the electron mobility of P(NDI2OD-T2) spin-coated films is enhanced by 2 orders of magnitude by simply using solvents that induce a high amount of preaggregates in solution, thus resulting in an extended order of domains in the copolymer film.

■ ASSOCIATED CONTENT

Supporting Information

Derivation of the analytical expressions of relative infrared absorption intensities of C═O stretchings (a and b bands) (S1) and of OPLA (c band) (S2) in IRA-TR and RAIRS experiments; sketches of regular polymer structures (S3). This material is available free of charge via Internet.

■ AUTHOR INFORMATION

Corresponding Authors

*E-mail: fazzi@mpi-muelheim.mpg.de.

*E-mail: chiara.castiglioni@polimi.it.

Notes

The authors declare no competing financial interest.

■ REFERENCES

(1) Zhan, X.; Facchetti, A.; Barlow, S.; Marks, T. J.; Ratner, M. A.; Wasielewski, M. R.; Marder, S. R. Rylene and Related Diimides for Organic Electronics. *Adv. Mater.* **2011**, *23*, 268−284.

(2) Sirringhaus, H. Reliability of Organic Field-Effect Transistors. *Adv. Mater.* **2009**, *21*, 3859−3873.

(3) Sakanoue, T.; Sirringhaus, H. Band-like Temperature Dependence of Mobility in a Solution-Processed Organic Semiconductor. *Nat. Mater.* **2010**, *9*, 736−740.

(4) Facchetti, A. π-Conjugated Polymers for Organic Electronics and Photovoltaic Cell Applications. *Chem. Mater.* **2011**, *23*, 733−758.

(5) Usta, H.; Facchetti, A.; Marks, T. J. n-Channel Semiconductor Materials Design for Organic Complementary Circuits. *Acc. Chem. Res.* **2011**, *44*, 501−510.

(6) Wang, C.; Dong, H.; Hu, W.; Liu, Y.; Zhu, D. Semiconducting π-Conjugated Systems in Field-Effect Transistors: A Material Odyssey of Organic Electronics. *Chem. Rev.* **2011**, *112*, 2208−2267.

(7) Ghezzi, D.; Antognazza, M. R.; Dal Maschio, M.; Lanzarini, E.; Benfenati, F.; Lanzani, G. A Hybrid Bioorganic Interface for Neuronal Photoactivation. *Nat. Commun.* **2011**, *2*, 166.

(8) Rauch, T.; Boberl, M.; Tedde, S. F.; Furst, J.; Kovalenko, M. V.; Hesser, G.; Lemmer, U.; Heiss, W.; Hayden, O. Near-Infrared Imaging with Quantum-dot-sensitized Organic Photodiodes. *Nat. Photonics* **2009**, *3*, 332−336.

(9) Akkerman, H. B.; Blom, P. W. M.; de Leeuw, D. M.; de Boer, B. Towards Molecular Electronics with Large-Area Molecular Junctions. *Nature* **2006**, *441*, 69−72.

(10) Mas-Torrent, M.; Rovira, C. Role of Molecular Order and Solid-State Structure in Organic Field-Effect Transistors. *Chem. Rev.* **2011**, *111*, 4833−4856.

(11) Arias, A. C.; MacKenzie, J. D.; McCulloch, I.; Rivnay, J.; Salleo, A. Materials and Applications for Large Area Electronics: Solution-Based Approaches. *Chem. Rev.* **2010**, *110*, 3−24.

(12) Li, C.; Liu, M.; Pschirer, N. G.; Baumgarten, M.; Müllen, K. Polyphenylene-Based Materials for Organic Photovoltaics. *Chem. Rev.* **2010**, *110*, 6817−6855.

(13) Boudreault, P.-L. T.; Najari, A.; Leclerc, M. Processable Low-Bandgap Polymers for Photovoltaic Applications. *Chem. Mater.* **2010**, *23*, 456−469.

(14) Lin, P.; Yan, F. Organic Thin-Film Transistors for Chemical and Biological Sensing. *Adv. Mater.* **2012**, *24*, 34−51.

(15) Soci, C.; Hwang, I. W.; Moses, D.; Zhu, Z.; Waller, D.; Gaudiana, R.; Brabec, C. J.; Heeger, A. J. Photoconductivity of a Low-Bandgap Conjugated Polymer. *Adv. Funct. Mater.* **2007**, *17*, 632−636.
(16) Moonen, P. F.; Yakimets, I.; Huskens, J. Fabrication of Transistors on Flexible Substrates: From Mass-Printing to High-Resolution Alternative Lithography Strategies. *Adv. Mater.* **2012**, *24*, 5526−5541.
(17) Carmen Ruiz Delgado, M.; Pigg, K. R.; da Silva Filho, D. A.; Gruhn, N. E.; Sakamoto, Y.; Suzuki, T.; Osuna, R. M.; Casado, J.; Hernández, V.; Navarrete, J. T. L.; et al. Impact of Perfluorination on the Charge-Transport Parameters of Oligoacene Crystals. *J. Am. Chem. Soc.* **2009**, *131*, 1502−1512.
(18) Di Pietro, R.; Fazzi, D.; Kehoe, T. B.; Sirringhaus, H. Spectroscopic Investigation of Oxygen- and Water-Induced Electron Trapping and Charge Transport Instabilities in n-type Polymer Semiconductors. *J. Am. Chem. Soc.* **2012**, *134*, 14877−14889.
(19) de Leeuw, D. M.; Simenon, M. M. J.; Brown, A. R.; Einerhand, R. E. F. Stability of n-type Doped Conducting Polymers and Consequences for Polymeric Microelectronic Devices. *Synth. Met.* **1997**, *87*, 53−59.
(20) Pearson, R. G. Ionization Potentials and Electron Affinities in Aqueous Solution. *J. Am. Chem. Soc.* **1986**, *108*, 6109−6114.
(21) Ponce Ortiz, R.; Herrera, H.; Mancheño, M. J.; Seoane, C.; Segura, J. L.; Burrezo, P. M.; Casado, J.; Navarrete, J. T. L.; Facchetti, A.; Marks, T. J. Molecular and Electronic-Structure Basis of the Ambipolar Behavior of Naphthalimide−Terthiophene Derivatives: Implementation in Organic Field-Effect Transistors. *Chem.—Eur. J.* **2013**, *19*, 12458−12467.
(22) Luzio, A.; Fazzi, D.; Natali, D.; Giussani, E.; Baeg, K.-J.; Chen, Z.; Noh, Y.-Y.; Facchetti, A.; Caironi, M. Synthesis, Electronic Structure, and Charge Transport Characteristics of Naphthalenediimide-Based Co-Polymers with Different Oligothiophene Donor Units. *Adv. Funct. Mater.* **2014**, *24*, 1151−1162.
(23) Sommer, M. Conjugated Polymers Based on Naphthalene Diimide for Organic Electronics. *J. Mater. Chem. C* **2014**, *2*, 3088−3098.
(24) Chen, Z.; Zheng, Y.; Yan, H.; Facchetti, A. Naphthalenedicarboximide- vs Perylenedicarboximide-Based Copolymers. Synthesis and Semiconducting Properties in Bottom-Gate N-Channel Organic Transistors. *J. Am. Chem. Soc.* **2009**, *131*, 8−9.
(25) Yan, H.; Chen, Z.; Zheng, Y.; Newman, C.; Quinn, J. R.; Dotz, F.; Kastler, M.; Facchetti, A. A High-Mobility Electron-Transporting Polymer for Printed Transistors. *Nature* **2009**, *457*, 679−686.
(26) Fazzi, D.; Caironi, M.; Castiglioni, C. Quantum-Chemical Insights into the Prediction of Charge Transport Parameters for a Naphthalenetetracarboxydiimide-Based Copolymer with Enhanced Electron Mobility. *J. Am. Chem. Soc.* **2011**, *133*, 19056−19059.
(27) Caironi, M.; Bird, M.; Fazzi, D.; Chen, Z.; Di Pietro, R.; Newman, C.; Facchetti, A.; Sirringhaus, H. Very Low Degree of Energetic Disorder as the Origin of High Mobility in an *n*-channel Polymer Semiconductor. *Adv. Funct. Mater.* **2011**, *21*, 3371−3381.
(28) Rivnay, J.; Mannsfeld, S. C. B.; Miller, C. E.; Salleo, A.; Toney, M. F. Quantitative Determination of Organic Semiconductor Microstructure from the Molecular to Device Scale. *Chem. Rev.* **2012**, *112*, 5488−5519.
(29) Sciascia, C.; Martino, N.; Schuettfort, T.; Watts, B.; Grancini, G.; Antognazza, M. R.; Zavelani-Rossi, M.; McNeill, C. R.; Caironi, M. Sub-Micrometer Charge Modulation Microscopy of a High Mobility Polymeric n-Channel Field-Effect Transistor. *Adv. Mater.* **2011**, *23*, 5086−5090.
(30) D'Innocenzo, V.; Luzio, A.; Petrozza, A.; Fazzi, D.; Caironi, M. Nature of Charge Carriers in a High Electron Mobility Naphthalenediimide Based Semiconducting Copolymer. *Adv. Funct. Mater.* **2014**, *24*, 5584−5593.
(31) Steyrleuthner, R.; Schubert, M.; Howard, I.; Klaumünzer, B.; Schilling, K.; Chen, Z.; Saalfrank, P.; Laquai, F.; Facchetti, A.; Neher, D. Aggregation in a High-Mobility n-Type Low-Bandgap Copolymer with Implications on Semicrystalline Morphology. *J. Am. Chem. Soc.* **2012**, *134*, 18303−18317.
(32) Rivnay, J.; Toney, M. F.; Zheng, Y.; Kauvar, I. V.; Chen, Z.; Wagner, V.; Facchetti, A.; Salleo, A. Unconventional Face-On Texture and Exceptional In-Plane Order of a High Mobility n-Type Polymer. *Adv. Mater.* **2010**, *22*, 4359−4363.
(33) Takacs, C. J.; Treat, N. D.; Krämer, S.; Chen, Z.; Facchetti, A.; Chabinyc, M. L.; Heeger, A. J. Remarkable Order of a High-Performance Polymer. *Nano Lett.* **2013**, *13*, 2522−2527.
(34) Luzio, A.; Criante, L.; D'Innocenzo, V.; Caironi, M. Control of Charge Transport in a Semiconducting Copolymer by Solvent-Induced Long-Range Order. *Sci. Rep.* **2013**, *3*, 3425.
(35) Rivnay, J.; Steyrleuthner, R.; Jimison, L. H.; Casadei, A.; Chen, Z.; Toney, M. F.; Facchetti, A.; Neher, D.; Salleo, A. Drastic Control of Texture in a High Performance n-Type Polymeric Semiconductor and Implications for Charge Transport. *Macromolecules* **2011**, *44*, 5246−5255.
(36) Fabiano, S.; Musumeci, C.; Chen, Z.; Scandurra, A.; Wang, H.; Loo, Y. L.; Facchetti, A.; Pignataro, B. From Monolayer to Multilayer N-Channel Polymeric Field-Effect Transistors with Precise Conformational Order. *Adv. Mater.* **2012**, *24*, 951−956.
(37) Lemaur, V.; Muccioli, L.; Zannoni, C.; Beljonne, D.; Lazzaroni, R.; Cornil, J.; Olivier, J. Y. On the Supramolecular Packing of High Electron Mobility Naphthalene Diimide Copolymers: The Perfect Registry of Asymmetric Branched Alkyl Side Chains. *Macromolecules* **2013**, *46*, 8171−8178.
(38) Caddeo, C.; Fazzi, D.; Caironi, M.; Mattoni, A. Atomistic Simulations of P(NDI2OD-T2) Morphologies: From Single Chain to Condensed Phases. *J. Phys. Chem. B* **2014**, *118*, 12556−12565.
(39) Hu, Z.; Muls, B.; Gence, L.; Serban, D. A.; Hofkens, J.; Melinte, S.; Nysten, B.; Demoustier-Champagne, S.; Jonas, A. M. High-Throughput Fabrication of Organic Nanowire Devices with Preferential Internal Alignment and Improved Performance. *Nano Lett.* **2007**, *7*, 3639−3644.
(40) Hartmann, L.; Tremel, K.; Uttiya, S.; Crossland, E.; Kayunkid, N.; Ludwigs, S.; Vergnat, C.; Brinkmann, M. 2D Versus 3D Crystalline Order in Thin Films of Regioregular Poly(3-hexylthiophene) Oriented by Mechanical Rubbing and Epitaxy. *Adv. Funct. Mater.* **2011**, *21*, 4047−4057.
(41) Brinkmann, M.; Rannou, P. Effect of Molecular Weight on the Structure and Morphology of Oriented Thin Films of Regioregular Poly(3-hexylthiophene) Grown by Directional Epitaxial Solidification. *Adv. Funct. Mater.* **2007**, *17*, 101−108.
(42) Heil, H.; Finnberg, T.; von Malm, N.; Schmechel, R.; von Seggern, H. The Influence of Mechanical Rubbing on the Field-Effect Mobility in Polyhexylthiophene. *J. Appl. Phys.* **2003**, *93*, 1636−1641.
(43) Derue, G.; Serban, D.; Leclere, P.; Melinte, S.; Damman, P.; Lazzaroni, R. Controlled Nanorubbing of Polythiophene Thin Films for Field-Effect Transistors. *Org. Electron.* **2008**, *9*, 821−828.
(44) Brinkmann, M.; Gonthier, E.; Bogen, S.; Tremel, K.; Ludwigs, S.; Hufnagel, M.; Sommer, M. Segregated versus Mixed Interchain Stacking in Highly Oriented Films of Naphthalene Diimide Bithiophene Copolymers. *ACS Nano* **2012**, *6*, 10319−10326.
(45) Giussani, E.; Fazzi, D.; Brambilla, L.; Caironi, M.; Castiglioni, C. Molecular Level Investigation of the Film Structure of a High Electron Mobility Copolymer via Vibrational Spectroscopy. *Macromolecules* **2013**, *46*, 2658−2670.
(46) Kline, R. J.; McGehee, M. D.; Toney, M. F. Highly Oriented Crystals at the Buried Interface in Polythiophene Thin-Film Transistors. *Nat. Mater.* **2006**, *5*, 222−228.
(47) Salleo, A.; Kline, R. J.; DeLongchamp, D. M.; Chabinyc, M. L. Microstructural Characterization and Charge Transport in Thin Films of Conjugated Polymers. *Adv. Mater.* **2010**, *22*, 3812−3838.
(48) Joshi, S.; Pingel, P.; Grigorian, S.; Panzner, T.; Pietsch, U.; Neher, D.; Forster, M.; Scherf, U. Bimodal Temperature Behavior of Structure and Mobility in High Molecular Weight P3HT Thin Films. *Macromolecules* **2009**, *42*, 4651.
(49) Tremel, K.; Fischer, F. S. U.; Kayunkid, N.; Di Pietro, R.; Kiriy, A.; Neher, D.; Ludwigs, S.; Brinkmann, M. Charge Transport Anisotropy in Highly Oriented Thin Films of the Acceptor Polymer

P(NDI2OD-T2). *Adv. Energy Mater.* **2014**, DOI: 10.1002/aenm.201301659.

(50) Fornari, R.; Troisi, A. Theory of Charge Hopping along a Disordered Polymer Chain. *Phys. Chem. Chem. Phys.* **2014**, *16*, 9997−10007.

(51) Liu, T.; Troisi, A. Understanding the Microscopic Origin of the Very High Charge Mobility in PBTTT: Tolerance of Thermal Disorder. *Adv. Funct. Mater.* **2014**, *24*, 925−933.

(52) Qin, T.; Troisi, A. Relation between Structure and Electronic Properties of Amorphous MEH-PPV Polymers. *J. Am. Chem. Soc.* **2013**, *135*, 11247−11256.

(53) The discussion is based on the following hypothesis: The total absorption intensity associated with CH stretching modes localized on the side alkyl chains is scarcely sensitive to the polymer orientation. This hypothesis comes from the observation that these chains exhibit a rather complex structure showing different relative orientation (ref 33) even in highly ordered 3-D crystal packing. As a consequence, the intensity of IR features associated with methylene groups is expected to be similar to that found for a disordered system, and thus quite insensitive to the polarization of the radiation field.

(54) Chambers, J. M.; Griffiths, P. R. *Handbook of Vibrational Spectroscopy*; John Wiley and Sons Ltd.: Chichester, West Sussex, UK, 2002; Vol. *2*.

(55) DFT geometry optimizations predict four different τ values: $\tau = \pm 42^\circ, \pm 138^\circ$ corresponding to pairs of two equivalent *syn* and *anti* conformations.[45] Our model cannot distinguish between the two pairs, so the analysis is restricted to $\tau = \pm 42^\circ$. The two values $\tau = 42^\circ$ and $\tau = 138^\circ = 180^\circ - 42^\circ$ correspond to two nonequivalent minima of the torsional potential energy surface of the NDI2OD-T2 unit. These minima are close in energy, and their structures are characterized by a different distance between the sulfur atom and the neighbor carbonyl group. From the equations in Table 2, the same relationships are obtained by substitution of τ with $\tau' = 180 + \tau$. In the subsequent discussion, $\tau = \pm 42^\circ$ simultaneously describes two different conformations, *anti* or *syn*.